Applied Catalysis B: Environmental 198 (2016) 171–179

Contents lists available at ScienceDirect

Applied Catalysis B: Environmental

journal homepage: www.elsevier.com/locate/apcatb

Facile synthesis of highly active Rh/Al_2O_3 steam reforming catalysts with preformed support by flame spray pyrolysis

Jiafeng Yu[a], Zhe Zhang[a], Felix Dallmann[b], Jixin Zhang[a], Dengyun Miao[a], Hengyong Xu[a], Andreas Goldbach[a,*], Roland Dittmeyer[b,*]

[a] Dalian National Laboratory for Clean Energy, Dalian Institute of Chemical Physics, Chinese Academy of Sciences, Dalian, China
[b] Institute for Micro Process Engineering, Karlsruhe Institute of Technology, Karlsruhe, Germany

ARTICLE INFO

Article history:
Received 12 February 2016
Received in revised form 6 May 2016
Accepted 20 May 2016
Available online 20 May 2016

Keywords:
Rh/Al_2O_3
Flame spray pyrolysis
Preformed support
Methane steam reforming
Turnover frequency

ABSTRACT

A highly active catalyst is a necessity for a compact microchannel membrane reactor for methane steam reforming (MSR) due to the limitation of catalyst loading per membrane area and the deliberately reduced working temperature compared to a conventional reformer. Two series of Rh/Al_2O_3 catalysts with nominal Rh loadings in the range of 0.2–5 wt.% were prepared by flame spray pyrolysis (FSP) using flame made and preformed support particles. For the flame made support, Rh and Al precursors were premixed and sprayed simultaneously. In the other case, the Rh precursor was mixed with a preformed boehmite particle suspension and then sprayed into the flame. Their catalytic activity was investigated for MSR in a fix-bed reactor. The nominal 1 wt.% Rh catalyst supported on preformed Al_2O_3 exhibited the highest CH_4 conversion of all catalysts at $W/F = 0.374\ g_{cat}\ h/mol_{CH4}$ and 600 °C. The turnover frequency (TOF) over both types of catalysts was much higher than the values of reported Rh reforming catalysts in that temperature range. In addition, the TOF values of catalysts based on preformed Al_2O_3 particles exceeded those over the ones with in situ formed Al_2O_3 by 29–39%. It is proposed that the preformed Al_2O_3 support promotes the catalytic activity, possibly enhancing H_2 spillover which is considered to facilitate the rate determining steps in MSR. The successful synthesis of catalysts supported by preformed materials opens new possibilities for preparation of nano-structured catalysts from a multitude of support materials via flame spray pyrolysis.

1. Introduction

Hydrogen is not only an important chemical feedstock but also a clean energy carrier. Natural gas as a global energy source has been gaining wide spread attention in recent years as a result of the growing global awareness of environmental issues [1]. In this context, natural gas steam reforming plays an important role in hydrogen production [2]. The major chemical reactions are steam reforming of methane (MSR) followed by the water-gas shift reaction (WGS). The overall reaction is an endothermic, equilibrium limited reaction [3]:

$$CH_4 + 2\,H_2O \leftrightarrows CO_2 + 4\,H_2,\ \Delta H_{298K} = 165\ kJ/mol \quad (1)$$

Generally, methane reforming is conducted industrially over a Ni-based catalyst at temperatures above 800 °C in a packed bed tubular reactor. The reactor tubes are heated by gas-fired burners. Due to the high endothermicity of the reaction and the large dimensions of the tubes, the process is heat transfer limited, which results in large temperature gradients in the packed bed in axial and radial direction. Microchannel reactors allow excellent temperature control and can also improve mass transport especially when dealing with highly exothermic and endothermic reactions [4–7]. Moreover, the integration of a Pd membrane in a steam reformer enables a shift of the chemical equilibrium as a consequence of hydrogen removal from the reaction zone and thus lowering of the reaction temperature to less than 600 °C [3,8–10]. However, the amount of catalyst is restricted by the limited space in microchannels, which makes it difficult to balance the local rates of hydrogen production and hydrogen removal [7]. A major challenge in this application is the insufficient activity of currently used steam reforming catalyst at such low temperatures. Therefore noble metal-based catalysts are considered instead, such as Ru, Pt and Rh, which also offer better resistance against carbon deposition than Ni-based catalysts [11–13]. High loadings of Rh (10–15 wt.%) have been deposited on preformed alumina layers in microchannels by impregnation and

* Corresponding authors.
E-mail addresses: goldbach@dicp.ac.cn (A. Goldbach), roland.dittmeyer@kit.edu (R. Dittmeyer).

http://dx.doi.org/10.1016/j.apcatb.2016.05.050
0926-3373/

proved to be efficient for methane steam reforming in microreactors in previous studies as they maximize the productivity per area of coated wall [14–16]. However, the metal dispersion is limited at high loadings leading to a poor utilization of the expensive noble metals. Therefore, we are interested in nano-sized catalysts with high metal dispersion to decrease the noble metal loading.

In recent years, flame spray pyrolysis (FSP) has become a versatile technique for preparing nano-sized crystalline materials in one step with high surface area and high metal dispersion and without any additional drying and calcination steps [17,18]. Catalyst metal and support precursors are sprayed into a flame and decompose simultaneously forming particles that are rapidly quenched using a cooled collector. The short residence time at elevated temperatures (up to 2000 °C [19]) is advantageous as it prevents significant sintering of the noble metals on the support and preserves nano-sized metal particles which also show excellent thermal stability [20]. Nano-sized Rh particles (1–2 nm) were successfully deposited on Al_2O_3 by the FSP method before and the resulting materials showed high catalytic performance in partial oxidation of methane [21]. However, incorporation of the active phase into the oxide support or composite formation may occur during single-nozzle flame spray pyrolysis, which then leads to a loss of accessible active centers [22–25].

The aim of the present study is to improve the metal distribution on the support in flame-made Rh/Al_2O_3 catalysts in order to prevent the encapsulation of catalytically active Rh centers by the support phase. For that purpose, we have synthesized two series of Rh/Al_2O_3 catalysts by FSP: One with Rh nanoclusters deposited on alumina particles generated directly in the flame and one with Rh deposited on preformed support particles injected into the flame. We also varied the Rh loading to better understand the Rh distribution on these catalysts and its effect on catalytic performance in MSR.

2. Experimental

2.1. Catalyst preparation

The scheme of the FSP setup used for this study was described elsewhere [26]. A flame generator (NanoPowder Nozzle npn) and a collection cylinder were purchased from Tethis S.p.A. The flame was generated by burning a mixture of CH_4 and O_2 which were fed with flow rates of 0.6 l/min and 1.9 l/min, respectively. The metal precursor solution was supplied to the flame at a flow rate of 5 ml/min by a syringe pump (PHD Ultra™, Harvard). Additional dispersion gas (O_2) was fed through the gap around the precursor solution nozzle (feed rate 3.5 l/min, pressure 4.5 bar). In order to stabilize the flame, additional 5 l/min oxygen was provided through a sintered metal plate ring as sheath for the supporting flame. The product particles were collected on a water-cooled glass fiber filter (Whatman GF/D, 25.7 cm in diameter) with the aid of a vacuum pump. Two lines of cooling water were used to control the temperature of the flame nozzle and the filter. The deposited particles were collected carefully from the filter after cooling down the FSP system.

Flame-made Rh/Al_2O_3 catalysts with Rh loadings of 0.2–5 wt.% were prepared by dissolving the appropriate amounts of Rh and Al precursor in a 1:1:2 (volume ratio) mixture of acetic acid (AA), 2-ethylhexanoic acid (EHA) and methanol (MeOH). The Al metal concentration was always 0.5 M. Two different alumina supports were used in this work. Flame made Al_2O_3 (denoted FAl) was formed directly during FSP from a precursor mixture that consisted of Rh acetylacetonate (Premion, 99.99%) and Al acetylacetonate (Merck). The other Al_2O_3 support was based on a preformed alumina particle suspension (Alfa Aesar, 20 wt.% stabilized alumina in water) and is therefore denoted SAl. This suspension was mixed with the Rh acetylacetonate precursor (in 1:1:2 AA/EHA/MeOH solution) and then sprayed into the flame. The Rh-based catalysts with flame made and suspension based supports are denoted as xRh/FAl and xRh/SAl, respectively, where x represents the targeted Rh loading in wt.%.

2.2. Catalyst characterization

The chemical composition of the produced catalysts was determined by inductively coupled plasma optical emission spectroscopy (ICP-OES, PerkinElmer 7300DV). The samples (10 mg) were chemically digested by dissolution in a mixture of 15 ml HCl and 5 ml HNO_3 in an autoclave for 2 h at 150 °C. X-ray powder diffraction (XRD) patterns of the prepared samples were measured on an X'Pert Pro (PANAlytical) diffractometer with Cu Kα radiation at 40 kV and 40 mA. The specific surface area of the catalysts was analyzed by nitrogen adsorption/desorption at −196 °C using the BET method (Quantachrome Autosorb iQ2).

Pulse chemisorption of H_2 was performed on an automatic analyzer (Micromeritics Autochem 2910) to determine the Rh dispersion in the different catalysts. A certain amount of sample was filled in a reactor and reduced in pure H_2 (30 ml/min) at 400 °C for 1 h. After reduction, the samples were purged with Ar (30 ml/min) at the same temperature for 1 h and then cooled down to 30 °C. Exact 1 ml pulses of a mixture of 10 vol.% H_2 in Ar were delivered to the reactor at 4 min intervals. The Rh dispersion was calculated from the cumulative volume of H_2 adsorbed from all pulses and the Rh loading determined by ICP assuming an adsorption stoichiometry of H:Rh = 1:1 [27]. The following relationship for spherical particles has been used to derive average Rh particle sizes from metal dispersions [28]:

$$D = 6\frac{\nu_m/a_m}{d} \quad (2)$$

where D is the metal dispersion, ν_m is the volume occupied by an atom in the bulk metal, a_m is the area occupied by a surface atom and d is the particle diameter. The values of ν_m and a_m for Rh are 13.78 Å^3 and 7.58 Å^2, respectively [29].

Temperature programmed reduction with hydrogen (H_2-TPR) was carried out in a homemade setup consisting of a quartz reactor in a temperature-programmable furnace and a thermo conductivity detector (TCD) for analysis. All catalysts were pretreated in air at 400 °C for 6 h before TPR measurement to remove residual carbonaceous species from the organic precursors following literature procedures [30]. After the pretreatment, the samples (40 mg) were loaded into the quartz reactor and in situ treated in a dry Ar stream (30 ml/min) at 300 °C for 0.5 h. After cooling down to room temperature, the furnace was heated to 600 °C with a temperature ramp of 10 °C/min in a mixture of 5 vol.% H_2 in Ar (30 ml/min).

Before transmission electron microscopy (TEM) examination, the samples were reduced at 400 °C in pure H_2 for 1 h and ultrasonically suspended in ethanol for 10 min. Then a drop of the resulting suspension was placed on a holey carbon film supported by a TEM copper grid. TEM images were acquired using a JEOL JEM-2100 system with an acceleration voltage of 200 kV. High-angle annular dark field scanning transmission electron microscope (HAADF-STEM) images were obtained on a JEOL JEM-ARM200F instrument equipped with a CEOS probe corrector.

2.3. Catalytic tests

The methane steam reforming experiments were performed using a tubular quartz reactor in a homemade setup decsribed elsewhere [31]. A mixture of 40 mg catalyst powder (40–60 mesh particle size) and quartz sand of similar size as diluent with a weight ratio of 2.5:1 (quartz/catalyst) was placed at the center of

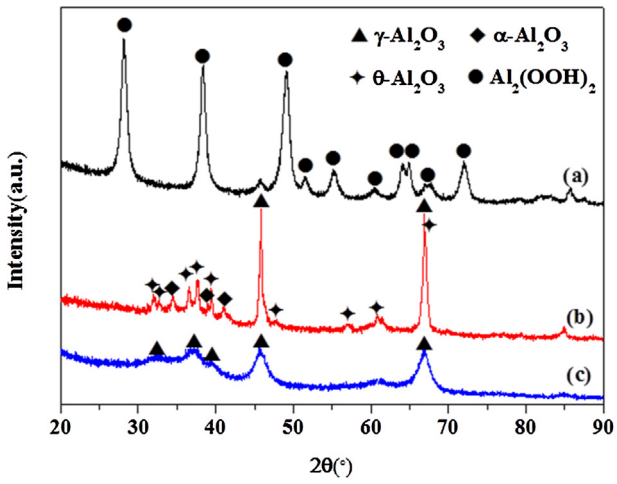

Fig. 1. XRD patterns of (a) the Al_2O_3 suspension precursor, (b) 5Rh/SAl and (c) 5Rh/FAl.

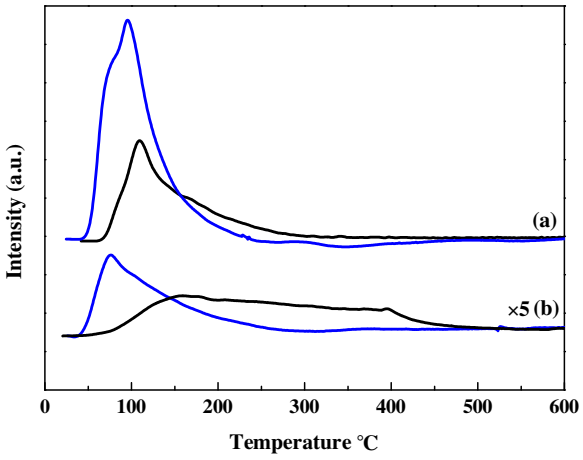

Fig. 2. TPR profiles of Rh-based catalysts with nominal Rh loadings of (a) 5% and (b) 1% supported on flame made Al_2O_3 (FAl, black) and preformed Al_2O_3 (SAl, blue). (For interpretation of the references to colour in this figure legend, the reader is referred to the web version of this article.)

the reactor. The sample was reduced in situ under pure H_2 (99.99%, 30 ml/min) at 400 °C for 0.5 h prior to the reaction. Methane steam reforming was conducted in the temperature range from 400 °C to 700 °C and 0.1 MPa with constant inlet concentrations of 10 vol.% CH_4, 40 vol.% H_2O, and 50 vol.% He, which corresponds to a steam-to-carbon ratio of 4 and a modified contact time (weight/flow ratio, W/F) of 0.374 g_{cat} h/mol_{CH4}. Note that the W/F ratio was calculated from the mass of catalyst divided by the molar flow of methane. The amount of catalyst was varied from 5 to 10 mg to limit CH_4 conversion to 20% at maximum for determination of reaction rates and TOF calculation. At each reaction temperature the CH_4 conversion was calculated based on the composition of the product gas after 1 h stabilization. Water was introduced with a high-pressure syringe pump (Elite P230) into a preheater zone maintained at 160 °C and vaporized into a He stream. The effluent from the reactor was analyzed using an automated Shimadzu GC-8A gas chromatograph equipped with TCD. The conversion of CH_4 (X_{CH4}, in %) was calculated according to

$$X_{CH4} = (1 - \frac{[CH4]_{out}}{[CH4]_{out}+[CO]_{out}+[CO2]_{out}}) \times 100 \quad (3)$$

where $[CH_4]_{out}$, $[CO]_{out}$ and $[CO_2]_{out}$ are the CH_4, CO and CO_2 concentrations in the product gas, respectively. The thermodynamic MSR equilibrium conversion $X_{CH4,eq}$ was calculated according to Eq. (3) replacing the outlet concentrations with equilibrium values determined by the program Gaseq (http://www.arcl02.dsl.pipex.com/). The turnover frequency (TOF) was calculated according to

$$TOF = \frac{\text{Moles of } CH_4 \text{ converted/second}}{\text{Moles of active Rh sites}} \quad (4)$$

where the moles of active Rh sites were derived from the H_2 chemisorption results.

3. Results and discussion

3.1. Morphological and structural properties of catalysts

The XRD patterns of 5Rh/FAl, 5Rh/SAl and the preformed Al_2O_3 particles without flame treatment are shown in Fig. 1. Rh related reflections were not detected in any of the samples indicating a small Rh particle size below the XRD detection limit (ca. 4 nm). For the 5Rh/FAl catalyst with in situ formed Al_2O_3, only the characteristic peaks of γ-Al_2O_3 were detected, indicating that the Al precursor aluminum (III) acetylacetonate got decomposed into γ-Al_2O_3 without further phase transformation during the FSP process. In general, phase transformation from γ- to α-Al_2O_3 via the intermediate δ- and θ-phases is completed above 1100 °C. [20]. The formation of the γ-phase in the high temperature flame could be explained by the fact that the Al_2O_3 particles spent only a few seconds in the flame. Formed particles were cooled down rapidly by the sheath gas and water-cooled collection filter at the top of the cylinder. Thus, the time at high temperature was too short for forming α-Al_2O_3 which was also reported by other researchers [32–34]. The Al_2O_3 particles in suspension were made of boehmite ($Al_2(OOH)_2$). After the FSP treatment two sharp peaks of γ-Al_2O_3 were found. Significant amounts of the intermediate θ- and high-temperature α-phases were also detected, indicating that high-temperature phases formed more easily with that support precursor. Moreover, the average FAl and SAl crystal sizes were about 9 and 34 nm, respectively, as calculated from the XRD patterns according to Scherrer's formula.

The TPR results are shown in Fig. 2. The reduction features are very weak for the catalysts with 0.2% Rh (not shown), but strong H_2 consumption peaks were observed around 100 °C for the catalysts with 1% and 5% Rh in agreement with literature results for Rh-based catalysts [35,36]. In general, the reduction temperature increased with decreasing Rh loading and was higher for FAl supported Rh catalysts than for the corresponding SAl supported ones. Evidently, Rh reduction is facilitated on the suspension based Al_2O_3.

The BET surface areas of FAl and SAl supports were 194 and 27 m^2/g, respectively. This large difference is a result of the differing Al_2O_3 particle size. The size of the Al_2O_3 particles in the suspension was 80–100 nm according to the manufacturer. According to TEM images, the SAl particle size distribution was a bit wider ranging from 50 to 200 nm. Therefore, the low surface area of SAl resulted from a relatively large particle size and the absence of intraparticle porosity. In contrast, the Al_2O_3 particle size was on the order of 10 nm for the FAl catalysts according to TEM results. Note also that the nitrogen adsorption–desorption isotherms of the flame made catalysts indicated that these materials did not have a well-defined mesoporous structure.

Scanning transmission electron microscopy was used for examination of the Rh nanoclusters on the supports, the determination of their morphology, and the analysis of the element distributions on the catalysts. STEM pictures of 5Rh/FAl and 5Rh/SAl are shown in Fig. 3(a) and (c), respectively. The Rh particles were discernible as bright, spherical dots on the spherical Al_2O_3 support particles. The FAl support exhibited a highly regular, sharp-edged structure with an average particle size of about 10 nm, which matched the

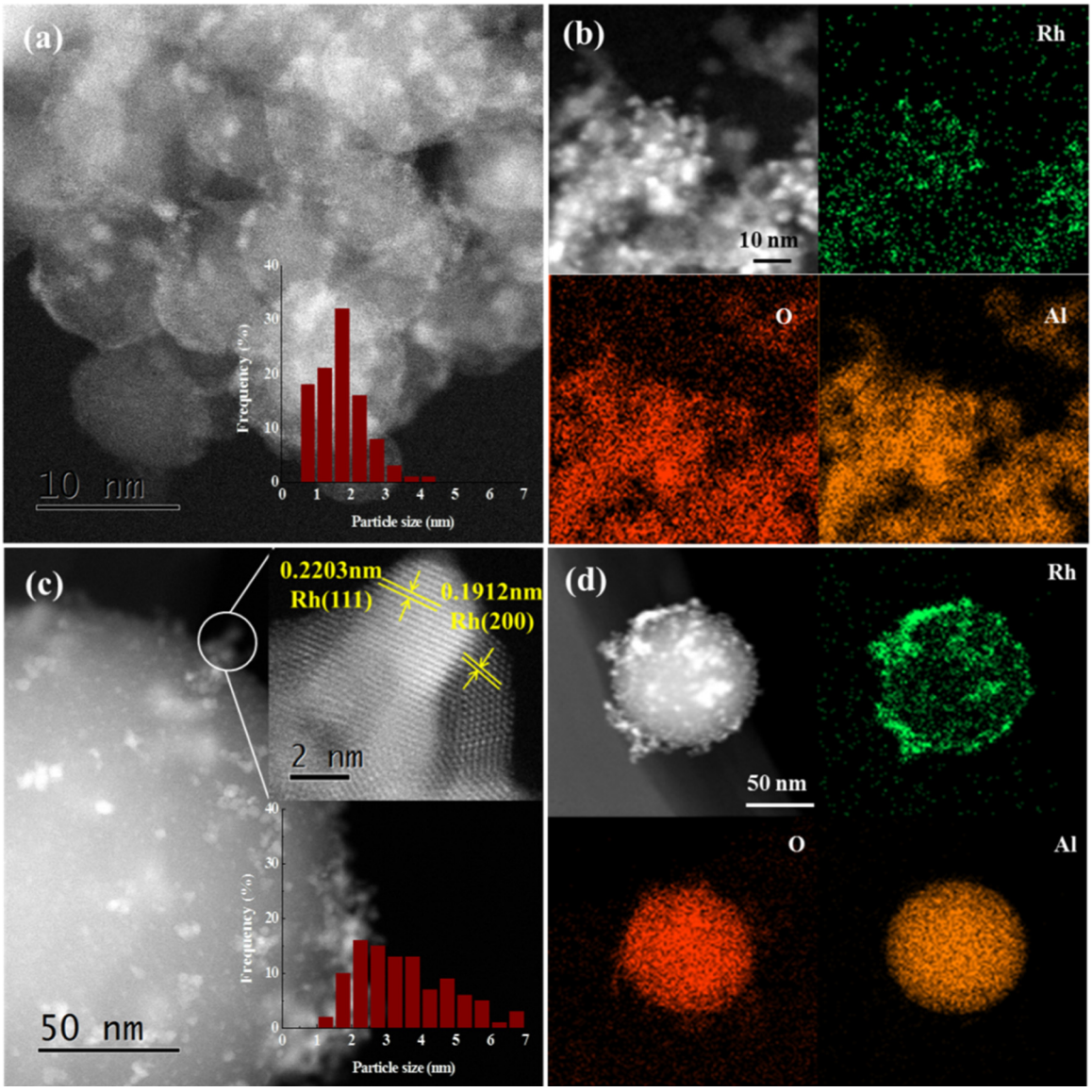

Fig. 3. HAADF-STEM images of flame made Rh/Al_2O_3 catalysts on different supports, pre-reduced at 400 °C: (a, b) 5Rh/FAl and (c, d) 5Rh/SAl with elemental mapping of Rh, O and Al (b, d); the lower insets in (a) and (c) show the Rh particle size distribution, and the upper inset in (c) a magnification of the marked area.

XRD result well. The inset of Fig. 3(a) shows that the Rh particles were distributed within a narrow size range from 1 to 3 nm and an average particle size of 1.6 nm according to the measurement of more than 100 Rh particles.

For 5Rh/SAl, it can be seen that the SAl support consisted of large spheres with a size in the range of 50–200 nm. In addition, small and large Rh particles were both restricted to the surface of the SAl support. The lattice distances of the clusters can be assigned to the Rh(111) and Rh(200) planes [36] and the Rh particles were distributed within a broader particle size range from 2 to 7 nm as shown in the insets of Fig. 3(c). The average Rh particle size on 5Rh/SAl was 3.5 nm from examination of the STEM images. Moreover, the elemental mapping of Rh, O and Al in 5Rh/FAl and 5Rh/SAl are shown in Fig. 3(b) and (d), respectively. Accordingly, Rh was uniformly and well dispersed on the FAl support. In contrast, many large Rh clusters were formed on the surface of the SAl particles which could be attributed to the high Rh loading and low surface area of this support.

High-resolution transmission electron microscopy (HRTEM) images of as-prepared 1Rh/FAl and 1Rh/SAl samples are shown in Fig. 4(a) and (c), respectively. Rather monodisperse Al_2O_3 spheres were also found in 1Rh/FAl with a particle size of about 10 nm which is consistent with the STEM observations for 5Rh/FAl. Rhodium particles were highly dispersed on 1Rh/FAl with a narrow distribution and an average particle size of 1.0 nm according to the measurement of more than 100 Rh particles. The Rh particles were also well dispersed on the surface of SAl with an average particle size of 1.7 nm. The lattice distances of the particle in the magnified image of the marked area of Fig. 3(c) agreed again well with the Rh(111) plane, indicating the presence of metallic Rh particles on the surface of SAl. It is worthwhile noting that no large Rh clusters could be detected on the SAl support in case of nominal Rh loadings lower than 1% which contrasts with the findings for 5Rh/SAl (Fig. 3). Therefore, we assume that the low surface area of the SAl support was insufficient for distributing the Rh well at 5% nominal loading, leading to the formation of large Rh clusters. The TEM images of the MSR-tested catalysts with 1% nominal Rh loading are shown in Fig. 4(b) and (d). The Rh particles had slightly grown to ca. 2 nm on both 1Rh/FAl and 1Rh/SAl after reaction according to the particle size distributions shown in the insets.

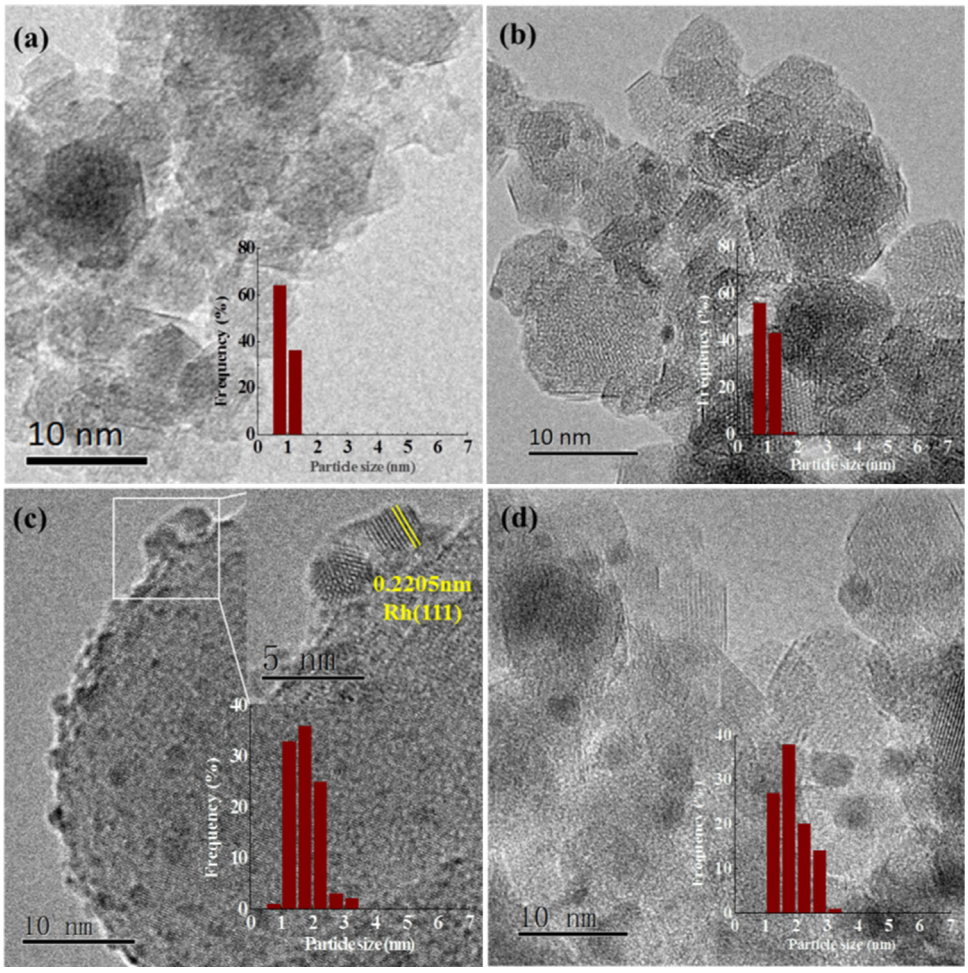

Fig. 4. HRTEM images of as-prepared 1Rh/FAl (a, b) and 1Rh/SAl (c, d) catalysts after reduction at 400 °C (a, c) as well as after MSR testing up to 600 °C (b, d); the insets are Rh particle size distributions with an additional magnification of the marked area in (c).

Table 1
Rh loading, H_2 chemisorption and TEM results of Rh/Al_2O_3 catalysts.

Catalyst	ICP-OES results	H_2 chemisorption results			TEM results	
	Rh loadings (%)	Rh active sites (A_{chem}) ($\mu mol/g_{cat}$)	Rh dispersion (%)	Rh particle size (P_{chem})[a] (nm)	Rh particle size (P_{TEM})[b] (nm)	Rh active sites (A_{TEM})[c] ($\mu mol/g_{cat}$)
5Rh/FAl	3.85	174	47	2.4	1.6	290
5Rh/SAl	2.75	117	44	2.5	3.5	90
1Rh/FAl	0.94	69	75	1.5	1.0	105
1Rh/SAl	0.84	59	73	1.5	1.7	53
0.2Rh/FAl	0.20	13	69	1.6	–	–
0.2Rh/SAl	0.20	12	61	1.8	–	–

[a] Calculated from metal dispersion measured by H_2 chemisorption according to Eq. (2).
[b] Measured Rh particles observed in TEM images.
[c] Calculated from the dispersion obtained from particle size (P_{TEM}) according to Eq. (2).

The characterization results from ICP, pulse H_2 chemisorption and TEM methods are summarized in Table 1. Rhodium particles could not be detected in TEM images of the catalysts with 0.2% Rh loading likely due to high Rh dispersion and small Rh amount. The Rh particle size was calculated from the Rh dispersion detected by H_2 chemisorption according to Eq. (2). The amount of Rh active sites was also derived from the Rh particle size observed by TEM using this equation. It can be seen from the H_2 chemisorption results that the Rh dispersion of the catalysts with 1% nominal Rh loading was higher than for the ones with 5% and 0.2% Rh loading for both FAl and SAl supported catalysts.

The Rh particle sizes derived from H_2 chemisorption (denoted as P_{chem}) were noticeably larger than the Rh particle sizes observed by TEM (denoted as P_{TEM}) for the FAl supported catalysts. In order to understand this discrepancy one needs to consider the limitations of both metal particle size analysis techniques. Hydrogen chemisorption can be misleading if strong metal-support interaction (SMSI), H_2 spillover, or reactive adsorption of H_2 on the support surface occur. The first phenomenon leads to an overestimation and the other two to an underestimation of the metal particle size. However, especially SMSI is not expected to be significant for the materials studied here. On the other hand, metal particles often cannot be detected by conventional TEM methods if they are very

small, metal concentrations are very low (as in the case of our samples with 0.2% Rh), or the contrast between metal and support is poor. In general, this leads to an overestimation of the average metal particle size and an underestimation of metal dispersion. In addition, only microscopic sample sections can be probed by TEM. Thus, variations in the macroscopic sample properties may not be fully captured. Also, TEM methods are not surface-sensitive, that is detected Rh particles may be covered by Al_2O_3. Such incorporated metal particles will not be accessible to H_2 or reactants, and accordingly, the number of catalytically active Rh sites can be overestimated on the basis of TEM analyses. Thus, the average metal particle size obtained by TEM has to be considered as an upper limit and derived active Rh site density too, if partial coverage of metal particles by the support is an issue.

With this in mind, the partial incorporation of Rh particles into the support is the most plausible explanation for the discrepancy between P_{chem} and P_{TEM} and related parameters for the FAl supported catalysts. Note that the incorporation of metals into the support is not unusual for single-nozzle flame made materials [23,25]. Because Al_2O_3-covered Rh particles were inaccessible to H_2, an overestimation resulted from the chemisorption method for the Rh particle size on the FAl catalysts. Accordingly, the number of Rh active sites derived from H_2 chemisorption (denoted as A_{chem}) was smaller than that calculated from TEM results (denoted as A_{TEM}). For example, A_{chem} = 174 μmol/g_{cat} while A_{TEM} = 290 μmol/g_{cat} for 5Rh/FAl. That suggests that ca. 40% of the present Rh sites were inaccessible due to the incorporation of Rh by Al_2O_3 during simultaneous formation of Rh and Al nanoparticles in the flame. Likewise, more than 30% of the Rh sites were lost in 1Rh/FAl due to coverage by Al_2O_3. However, only the metal particles accessible to reactants matter from a catalytic perspective. Therefore, the chemisorption-derived apparent values are the practically relevant ones for the Rh dispersion and the number of active Rh sites if specific reaction rates are to be determined.

In contrast, P_{chem} was similar or smaller than P_{TEM}, and A_{chem} was larger than A_{TEM} for SAl supported catalysts. As discussed above, larger P_{TEM} values could be due to Rh particles that are smaller than the TEM detection limit. However, it is also conceivable that H_2 spillover played a larger role on this support material leading to an underestimation of the Rh particle size which is not unusual for Rh-based catalysts [37,38]. Incorporation of Rh into the preformed Al_2O_3 particles is not expected for the SAl catalysts so that the Rh particles should be fully accessible to H_2 in those materials. Thus, the difference between A_{chem} = 117 μmol/g_{cat} and A_{TEM} = 90 μmol/g_{cat} may indicate that up to 30% of the H atoms adsorbed on 5Rh/SAl were not due to adsorption on Rh active sites but resulted from hydrogen spillover onto SAl.

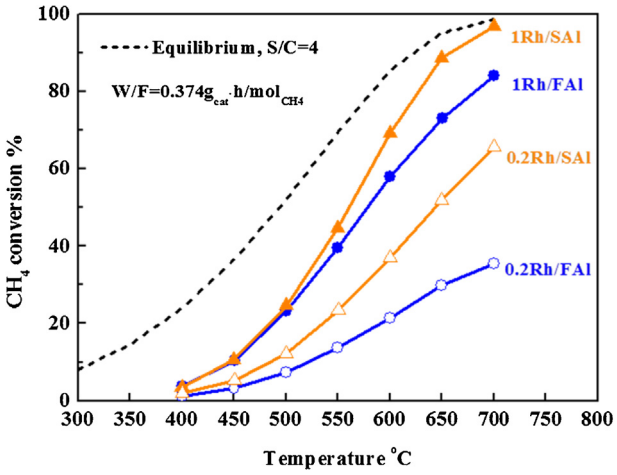

Fig. 5. CH_4 conversion during methane steam reforming over Rh/FAl and Rh/SAl catalysts with different Rh loading in the temperature range from 400 to 700 °C (0.1 MPa, steam/carbon ratio = 4, W/F = 0.374 g_{cat}·h/mol_{CH4}).

3.2. Catalytic properties

The CH_4 conversion is shown in Fig. 5 as a function of the reaction temperature for selected catalysts. The CH_4 conversion over the SAl supported catalysts was generally higher than that over the FAl supported catalysts, and the difference in activity increased with increasing temperature. This is consistent with the TPR results which showed that Rh on the preformed Al_2O_3 is more readily reduced and thus more reactive than Rh on the flame made Al_2O_3. In addition, H_2 spillover may have aided the conversion of CH_4 especially on SAl supported catalysts as indicated by the comparison of chemisorption and TEM results. Evidently, the nature of the Al_2O_3 support has a significant impact on the catalytic activity of these catalysts. 1Rh/SAl showed the best performance with CH_4 conversion approaching equilibrium conversion at 700 °C.

Methane conversions in Fig. 6(a) were determined at 600 °C, 0.1 MPa, steam/carbon ratio = 4 and W/F = 0.374 g_{cat} h/mol_{CH4}. The CH_4 conversion significantly increased from 21% to 58% when increasing the nominal Rh loading from 0.2% to 1% for the Rh/FAl catalysts. A further increase in Rh loading to 5% resulted only in little improvement from 58% to 65%. The Rh/SAl catalysts were more active than the corresponding Rh/FAl catalysts except for 5Rh/SAl which is simply a reflection of the ca. 40% higher Rh loading on the 5Rh/FAl catalyst. In order to demonstrate this effect of Rh loading on CH_4 conversion, we measured conversions at constant modified contact time W/F based on the actual mass of metallic Rh (W_{Rh}/F = 0.014 g_{Rh} h/mol_{CH_4}). As a result, the CH_4 conversion

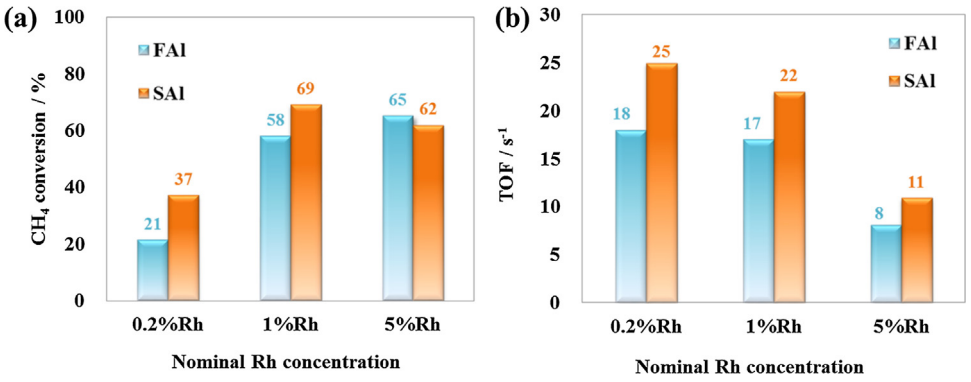

Fig. 6. Effect of Rh loading on (a) CH_4 conversion and (b) TOF for MSR on flame made Rh/Al_2O_3 catalysts supported by FAl (blue) and SAl (orange) at 600 °C. (For interpretation of the references to colour in this figure legend, the reader is referred to the web version of this article.)

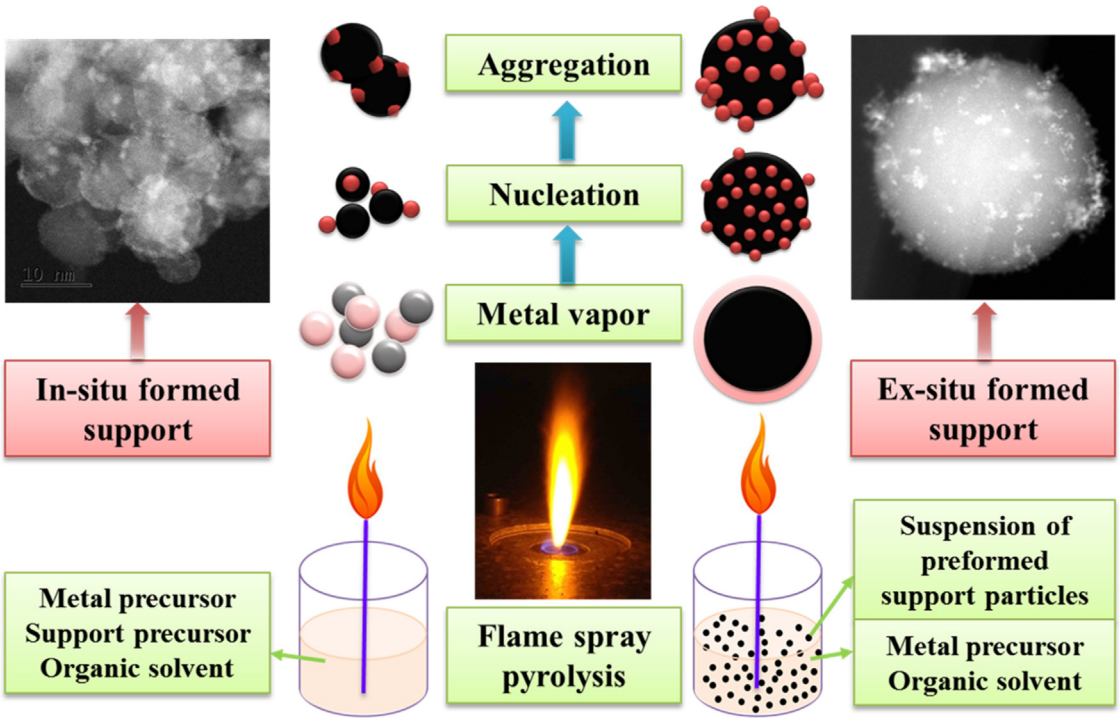

Fig. 7. Scheme of the gas-to-particle growth mechanism of catalyst formation with in situ and ex situ formed supports in the FSP process.

over 5Rh/SAl reached 81.1% which was much higher than the 65.2% obtained for 5Rh/FAl and in line with the findings for catalysts with lower Rh loading.

The 1Rh/SAl catalyst exhibited the highest activity of all samples, even higher than 5Rh/SAl and even though the amount of Rh active sites on 5Rh/SAl was higher than that on 1Rh/SAl. This may be attributed to the non-uniform distribution and larger Rh clusters on 5Rh/SAl (3.5 nm) compared to 1Rh/SAl (1.7 nm). It is known that small metal particles with a larger number of coordinatively unsaturated sites are more active for MSR than larger metal particles [39].

The turnover frequency (TOF) value enables a more instructive comparison of reactivity of catalysts with different Rh loadings. Hence the TOF values were calculated according to Eq. (4) and presented in Fig. 6(b). It can be seen that the TOF values increase with decreasing Rh loading. In addition, the TOF values of the SAl supported catalysts are always higher than those for the FAl supported catalysts exceeding the latter ones by 30–40%. This corroborates that the catalysts based on preformed Al_2O_3 particles were much more active than the ones on the in situ formed Al_2O_3 support. Our turnover frequencies are compared in Table 2 with corresponding values for methane steam reforming catalysts reported in the literature. In general, the relative MSR activity of metals follows the trend Pt > Ir > Pd > Rh > Ru > Ni [45]. It is obvious that our flame made catalysts rank among the top MSR Rh-based catalysts reported so far, exhibiting activities even comparable to highly active Pt/ZrO_2–CeO_2 catalysts [40]. The TOF values of the catalysts prepared here (Fig. 6b) increase with decreasing Rh loading as it has been found for the Pt/ZrO_2–CeO_2 catalysts (Table 2). It has been reported that the overall CH_4 reforming rate over Ir catalysts is not affected by the chemical identity of the support [39]. Unlike that result, the TOF values of FAl supported catalysts were clearly lower than those of SAl supported ones. This demonstrates that the nature and the formation process of the support affect the catalytic activity of flame made Rh catalysts.

Table 2
CH_4 turnover frequency (TOF) over noble metal catalysts in methane steam reforming.

Catalyst	Metal amount(wt.%)	Temperature(°C)	TOF(s^{-1})	Ref.
Pt/ZrO_2–CeO_2	0.2	600	24.7	[40]
Pt/ZrO_2–CeO_2	0.4	600	22.5	[40]
Pt/ZrO_2–CeO_2	0.8	600	19.5	[40]
Pt/ZrO_2–CeO_2	1.6	600	14.8	[40]
Ir/ZrO_2	0.8	600	12.4	[41]
Pd/CeO_2–Al_2O_3	0.5	510	4.7	[42]
Pd/ZrO_2	1.6	550	10.8	[43]
Ru/Al_2O_3	3.2	600	4.2	[44]
Ni/MgO	7.0	600	4.1	[45]
Rh-Ni/Al_2O_3	0.2	525	1.6	[46]
Rh/ZrO_2	0.1	600	9.0	[47]
Rh/Al_2O_3	0.2	600	5.5	[47]
Rh/FAl	0.2	600	17.8	This work
Rh/SAl	0.2	600	24.6	This work
Rh/FAl	0.9	600	17.1	This work
Rh/SAl	0.8	600	21.5	This work

Two tentative explanations are proposed here for the higher catalytic activity of the Rh/SAl catalysts. According to literature reports [48–51], hydrogenolysis, hydrogenation, and dehydrogenation reactions can be significantly enhanced by hydrogen spilling over from active centers to neighboring sites. Therefore, the SAl support might better promote hydrogen spillover from Rh to the support, which may enhance its catalytic activity. This was concluded previously when TOF values of Rh supported on mesocelluar silica foams had been found to increase with decreasing Rh loading and had been correlated with the amount of spilt-over hydrogen [38]. Accordingly, the steam reforming reaction might be promoted by hydrogen spillover through facilitation of the dehydrogenation steps in the reforming process such as CH_4 dissociation and decomposition of reaction intermediates on the active centers, which are considered as rate determining steps in MSR [47]. On the other hand, it has been proposed that metal particles with high concentration of coordinatively unsaturated sites are more active for C—H activation, resulting in higher steam reforming turnover rates

[39,40,52]. This is known as structure sensitivity of MSR [39,40,52]. In general, the density of certain types of active sites, such as steps or edges, increases with decreasing metal particle size. However, the partial incorporation of Rh particles into Al_2O_3 support may have greater influence on the activity than the particle size because it may decrease the amount of steps or edges sites and the density of accessible catalytic sites in Rh/FAl catalysts.

3.3. Gas-to-particle mechanism in FSP process

In the FSP process, the metal precursor is a combustible liquid that is turned into a metal vapor via spraying and decomposition in the flame, as presented schematically in Fig. 7. Particles are formed after precursor conversion to nuclei, and these grow by surface reaction and subsequent coalescence and aggregation into larger particles [18,53,54]. The synthesis process of a flame made support is shown in the left part of Fig. 7. First, the solution consisting of the Rh and Al precursors and an organic solvent is well mixed. Rh and Al vapor are simultaneously formed when this mixture is sprayed through the nozzle. Then Al oxide nucleation occurs and further aggregation into large particles takes place with deposition of Rh particles on the surface. In this process, partial or complete incorporation of Rh particles into the Al_2O_3 support is likely to occur to some degree.

However, the gas-to-particle growth process of catalysts with preformed (ex-situ formed) support is different, as shown in the right part of Fig. 7. The solution is composed of the Rh precursor, an organic solvent and a suspension of preformed Al_2O_3 particles. In this case, the Rh vapor homogeneously surrounds the Al_2O_3 particles. Then the Rh nuclei form and aggregate right on the surface of the Al_2O_3 particles. Here, the dispersion of Rh on the support depends on the concentration of the Rh precursor. With an increase of the Rh concentration in the flame, the Rh loading of the particles increases, leading to an accumulation of larger Rh particles, as observed in the 5Rh/SAl catalyst.

4. Conclusions

Two series of Rh-based catalysts were successfully synthesized by flame spray pyrolysis on flame made and preformed support particles to elucidate the factors that determine the catalytic activity of such catalysts in MSR. The 1Rh/SAl catalyst exhibited the highest CH_4 conversion of all catalysts at $W/F = 0.374\ g_{cat}\ h/mol_{CH_4}$ and 600 °C. In general, the TOF values were higher for catalysts supported on preformed Al_2O_3 compared to those on flame made Al_2O_3. They also exceeded the values of Rh catalysts reported in the literature. It was found that about a third of the Rh was incorporated into the Al_2O_3 support in Rh catalysts supported on flame made Al_2O_3, leading to the loss of accessible Rh active sites. In addition, Rh reduction and H_2 spillover were facilitated on the catalysts made with preformed Al_2O_3 particles showing that the support plays a significant role in the catalytic activity of Rh. Hence, the catalytic performance of flame made catalysts can be significantly enhanced through using preformed Al_2O_3 supports. The novel approach in FSP to use preformed support particles has been proven to be effective. Further development of this method should focus on the investigation of inherent properties of the supports.

Acknowledgements

The authors would like to acknowledge Prof. Jan-Dierk Grunwaldt for his kind suggestions and Dr. Shu Miao for the STEM investigations. The research leading to these results has received funding from the Helmholtz Association of German Research Centres and the Chinese Academy of Sciences through the External Cooperation Program (Helmholtz-CAS Joint Research Group on Integrated Catalytic Technologies for Efficient Hydrogen Production, Grants HCJRG 118 and GJHZ1304) and the National Natural Science Foundation of China (Grant 21306183).

References

[1] M. Ball, M. Wietschel, Int. J. Hydrogen Energy 34 (2009) 615–627.
[2] J.A. Ritter, A.D. Ebner, Sep. Sci. Technol. 42 (2007) 1123–1193.
[3] B. Dittmar, A. Behrens, N. Schödel, M. Rüttinger, T. Franco, G. Straczewski, R. Dittmeyer, Int. J. Hydrogen Energy 38 (2013) 8759–8771.
[4] J.D. Holladay, Y. Wang, E. Jones, Chem. Rev. 104 (2004) 4767–4790.
[5] U. Izquierdo, V.L. Barrio, J.F. Cambra, J. Requies, M.B. Güemez, P.L. Arias, G. Kolb, R. Zapf, A.M. Gutiérrez, J.R. Arraibi, Int. J. Hydrogen Energy 37 (2012) 7026–7033.
[6] C. Cao, N. Zhang, X. Chen, Y. Cheng, Chem. Eng. Sci. 137 (2015) 276–286.
[7] T. Boeltken, M. Belimov, P. Pfeifer, T.A. Peters, R. Bredesen, R. Dittmeyer, Chem. Eng. Process. 67 (2013) 136–147.
[8] J. Tong, Y. Matsumura, Appl. Catal. A: Gen. 286 (2005) 226–231.
[9] Y. Chen, Y. Wang, H. Xu, G. Xiong, Appl. Catal. B: Environ. 81 (2008) 283–294.
[10] Y. Chen, Y. Wang, H. Xu, G. Xiong, J. Membr. Sci. 322 (2008) 453–459.
[11] L. Zhou, Y. Guo, Q. Zhang, M. Yagi, H. Li, J. Chen, M. Sakurai, H. Kameyama, Catal. Commun. 10 (2008) 325–329.
[12] H.-S. Roh, D.K. Lee, K.Y. Koo, U.H. Jung, W.L. Yoon, Int. J. Hydrogen Energy 35 (2010) 1613–1619.
[13] A.L.Y. Tonkovich, B. Yang, S.T. Perry, S.P. Fitzgerald, Y. Wang, Catal. Today 120 (2007) 21–29.
[14] J. Thormann, P. Pfeifer, K. Schubert, U. Kunz, Chem. Eng. J. 135 (2008) 74–81.
[15] Y. Wang, Y.H. Chin, R.T. Rozmiarek, B.R. Johnson, Y. Gao, J. Watson, A.Y.L. Tonkovich, D.P. Vander Wiel, Catal. Today 98 (2004) 575–581.
[16] S. Lee, T. Boeltken, A.K. Mogalicherla, U. Gerhards, P. Pfeifer, R. Dittmeyer, Appl. Catal. A: Gen. 467 (2013) 69–75.
[17] G.L. Chiarello, M.V. Dozzi, M. Scavini, J.-D. Grunwaldt, E. Selli, Appl. Catal. B: Environ. 160–161 (2014) 144–151.
[18] W.Y. Teoh, R. Amal, L. Madler, Nanoscale 2 (2010) 1324–1347.
[19] L. Mädler, H.K. Kammler, R. Mueller, S.E. Pratsinis, J. Aerosol Sci. 33 (2002) 369–389.
[20] R. Strobel, S.E. Pratsinis, A. Baiker, J. Mater. Chem. 15 (2005) 605–610.
[21] A.J. Santis-Alvarez, R. Büchel, N. Hild, W.J. Stark, D. Poulikakos, Appl. Catal. A: Gen. 469 (2014) 275–283.
[22] M. Høj, K. Linde, T.K. Hansen, M. Brorson, A.D. Jensen, J.-D. Grunwaldt, Appl. Catal. A: Gen. 397 (2011) 201–208.
[23] M. Tepluchin, D.K. Pham, M. Casapu, L. Madler, S. Kureti, J.-D. Grunwaldt, Catal. Sci. Technol. 5 (2015) 455–464.
[24] M. Tepluchin, M. Casapu, A. Boubnov, H. Lichtenberg, D. Wang, S. Kureti, J.-D. Grunwaldt, ChemCatChem 6 (2014) 1763–1773.
[25] G.L. Chiarello, J.-D. Grunwaldt, D. Ferri, F. Krumeich, C. Oliva, L. Forni, A. Baiker, J. Catal. 252 (2007) 127–136.
[26] S. Lee, K. Schneider, J. Schumann, A.K. Mogalicherla, P. Pfeifer, R. Dittmeyer, Chem. Eng. Sci. 138 (2015) 194–202.
[27] N. van Vegten, D. Ferri, M. Maciejewski, F. Krumeich, A. Baiker, J. Catal. 249 (2007) 269–277.
[28] G. Bergeret, P. Gallezot, G. Ertl, H. Knözinger, F. Schüth, J. Weitkamp, Handbook of Heterogeneous Catalysis, Wiley-VCH, Weinheim, 2008, pp. 738–765.
[29] G. Cavusoglu, D. Miao, H. Lichtenberg, H.W.P. Carvalho, H. Xu, A. Goldbach, J.-D. Grunwaldt, Appl. Catal. A: Gen. 504 (2015) 381–390.
[30] R. Kydd, W.Y. Teoh, K. Wong, Y. Wang, J. Scott, Q.-H. Zeng, A.-B. Yu, J. Zou, R. Amal, Adv. Funct. Mater. 19 (2009) 369–377.
[31] D. Miao, A. Goldbach, H. Xu, ACS Catal. 6 (2016) 775–783.
[32] R. Strobel, W.J. Stark, L. Mädler, S.E. Pratsinis, A. Baiker, J. Catal. 213 (2003) 296–304.
[33] R. Strobel, F. Krumeich, W.J. Stark, S.E. Pratsinis, A. Baiker, J. Catal. 222 (2004) 307–314.
[34] S. Hannemann, J.-D. Grunwaldt, P. Lienemann, D. Günther, F. Krumeich, S.E. Pratsinis, A. Baiker, Appl. Catal. A: Gen. 316 (2007) 226–239.
[35] R. Burch, P.K. Loader, N.A. Cruise, Appl. Catal. A: Gen. 147 (1996) 375–394.
[36] J.M. Gatica, R.T. Baker, P. Fornasiero, S. Bernal, G. Blanco, J. Kašpar, J. Phys. Chem. B 104 (2000) 4667–4672.
[37] D. Panayotov, E. Ivanova, M. Mihaylov, K. Chakarova, T. Spassov, K. Hadjiivanov, Phys. Chem. Chem. Phys. 17 (2015) 20563–20573.
[38] L. Qian, W. Cai, L. Zhang, L. Ye, J. Li, M. Tang, B. Yue, H. He, Appl. Catal. B: Environ. 164 (2015) 168–175.
[39] J. Wei, E. Iglesia, Angew. Chem. Int. Ed. 43 (2004) 3685–3688.
[40] J.M. Ramallo-López, F.G. Requejo, A.F. Craievich, J. Wei, M. Avalos-Borja, E. Iglesia, J. Mol. Catal. A: Chem. 228 (2005) 299–307.
[41] J. Wei, E. Iglesia, Phys. Chem. Chem. Phys. 6 (2004) 3754–3759.
[42] L.S.F. Feio, C.E. Hori, S. Damyanova, F.B. Noronha, W.H. Cassinelli, C.M.P. Marques, J.M.C. Bueno, Appl. Catal. A: Gen. 316 (2007) 107–116.
[43] A. Yamaguchi, E. Iglesia, J. Catal. 274 (2010) 52–63.
[44] J. Wei, E. Iglesia, J. Phys. Chem. B 108 (2004) 7253–7262.
[45] J. Wei, E. Iglesia, J. Catal. 224 (2004) 370–383.
[46] E.C. Luna, A.M. Becerra, M.I. Dimitrijewits, React. Kinet. Catal. Lett. 67 (1999) 247–252.

[47] J. Wei, E. Iglesia, J. Catal. 225 (2004) 116–127.
[48] J.T. Miller, B.L. Meyers, F.S. Modica, G.S. Lane, M. Vaarkamp, D.C. Koningsberger, J. Catal. 143 (1993) 395–408.
[49] S. Xia, R. Nie, X. Lu, L. Wang, P. Chen, Z. Hou, J. Catal. 296 (2012) 1–11.
[50] N. Jiang, K.S.R. Rao, M.-J. Jin, S.-E. Park, Appl. Catal. A: Gen. 425–426 (2012) 62–67.
[51] J. Yu, Q. Ge, W. Fang, H. Xu, Int. J. Hydrogen Energy 36 (2011) 11536–11544.
[52] J. Wei, E. Iglesia, J. Phys. Chem. B 108 (2004) 4094–4103.
[53] R. Strobel, A. Alfons, S.E. Pratsinis, Adv. Powder Technol. 17 (2006) 457–480.
[54] R. Strobel, S.E. Pratsinis, J. Mater. Chem. 17 (2007) 4743–4756.